

Supporting Information

Tunable luminescence thermal stability in $\text{YV}_x\text{As}_{1-x}\text{O}_4:\text{Eu}^{3+}$ through the introduction of As^{5+} ions for remote temperature sensing applications

W. M. Piotrowski^{1†}, M. Kardach^{1†}, P. Sobierajska¹, A. Watras¹, J. M. Reeks¹, V. Kinzhylalo¹,
L. Marciniak^{1*} and R. J. Wiglusz^{1*}

Institute of Low Temperature and Structure Research, Polish Academy of Sciences, Okolna 2, 50-422 Wroclaw, Poland

Keywords: yttrium orthovanadate, yttrium orthoarsenate, nanosized, sensor, luminescence, nano-thermometry

*Corresponding authors:
E-mail: l.marciniak@intibs.pl; r.wiglusz@intibs.pl

The integral intensities of the Eu^{3+} bands to calculate LIR values were fitted with Mott-Seitz equation (Eq. S1):

$$I = \frac{I_0}{C \cdot \exp(-\frac{W}{k \cdot T}) + 1} \quad (\text{Eq. S1})$$

where: I – the intensity in temperature T, I_0 – the intensity in the initial temperature, W - the activation energy, k – Boltzmann constant, C – the dimensionless constant.

The average lifetime of the excited states of Eu^{3+} ions were calculated with the equation Eq. S2:

$$\tau_{avr} = \frac{A_1\tau_1^2 + A_2\tau_2^2}{A_1\tau_1 + A_2\tau_2} \quad (\text{Eq. S2a})$$

where: τ_1 , τ_2 – the average time, which is in accordance with the relation $\tau = t \cdot \ln(2)$ and A_1 , A_2 – amplitude, which are the parameters of the double exponential function:

$$y = y_0 + A_1 \cdot \exp\left(-\frac{x}{t_1}\right) + A_2 \cdot \exp\left(-\frac{x}{t_2}\right) \quad (\text{Eq. S2b})$$

Temperature determination uncertainty was calculated using Eq. S3:

$$\delta T = \frac{1}{S_R} \cdot \frac{\delta LIR}{LIR} \quad (\text{Eq. S3a})$$

where: S_R is the relative sensitivity and $\delta LIR/LIR$ determines the uncertainty of the LIR determination where $\delta LIR/LIR$ was determined as follows:

$$\frac{\delta LIR}{LIR} = \sqrt{\left(\frac{\delta I_{Eu(exc1)}}{I_{Eu(exc1)}}\right)^2 + \left(\frac{\delta I_{Eu(exc2)}}{I_{Eu(exc2)}}\right)^2} \quad (\text{Eq. S3b})$$

Thermal expansion coefficients were calculated using Eq. S4:

$$\alpha_a = \frac{\Delta a}{a} \cdot \frac{1}{\Delta T} \quad (\text{Eq. S4a})$$

$$\alpha_c = \frac{\Delta c}{c} \cdot \frac{1}{\Delta T} \quad (\text{Eq. S4b})$$

where a and c are the unit cell parameters and $\Delta a/\Delta c$ refers to the change in a/c value corresponding to the change of temperature ΔT .

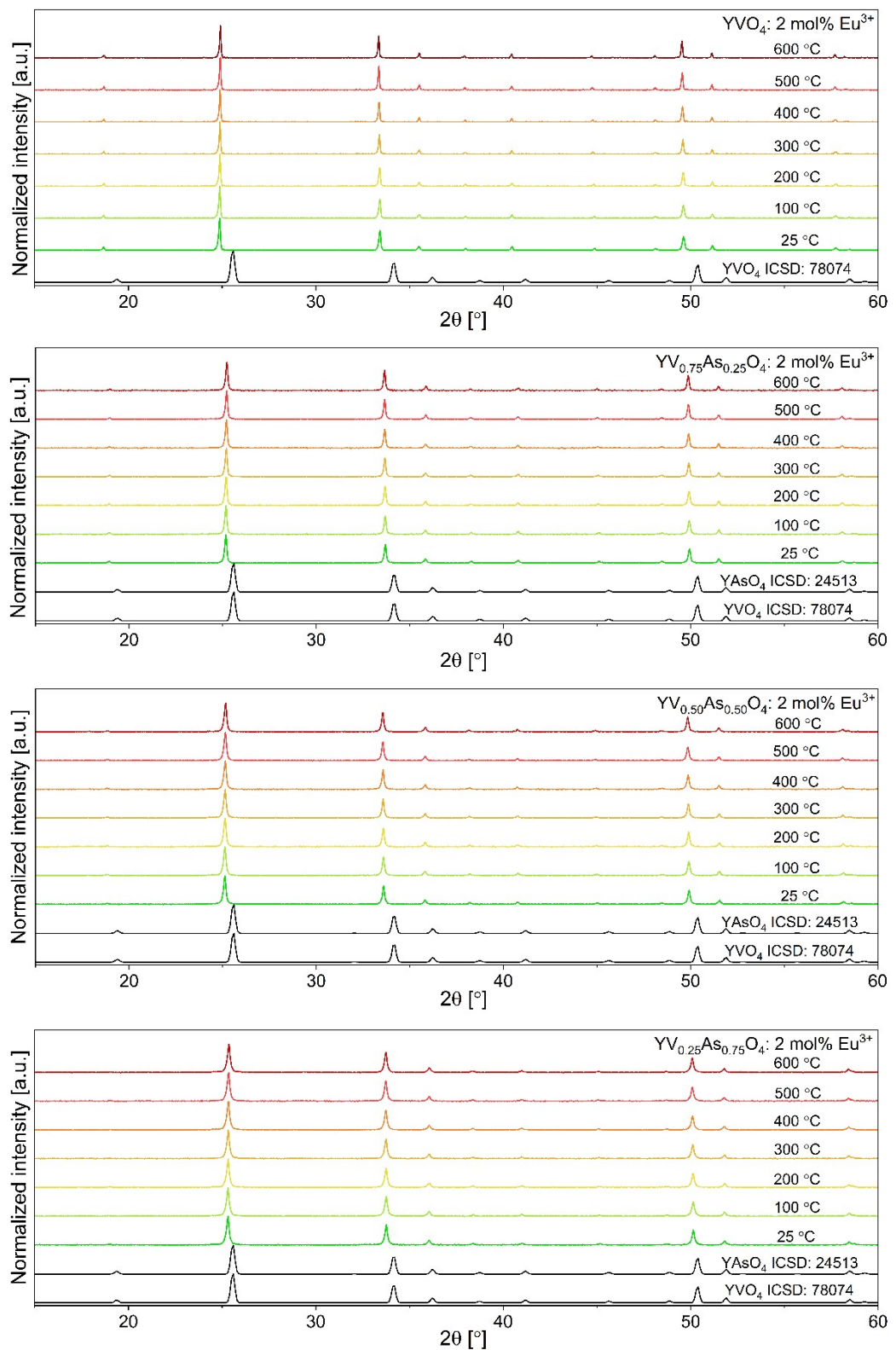


Figure S1. The X-ray diffractograms obtained for YVO_4 , $\text{YV}_{0.75}\text{As}_{0.25}\text{O}_4$, $\text{YV}_{0.50}\text{As}_{0.50}\text{O}_4$, and $\text{YV}_{0.25}\text{As}_{0.75}\text{O}_4$ doped with 2 mol% Eu^{3+} and measured at different temperatures.

Table S1. Influence of temperature on the unit cell parameters and cell volume in $\text{YV}_x\text{As}_{1-x}\text{O}_4$:2% Eu³⁺ materials.

YVO₄: 2% Eu³⁺	a [Å]	c [Å]	V [Å³]
298 K	7.1182(3)	6.2945(2)	318.9321
373 K	7.1196(3)	6.2986(2)	319.2732
473 K	7.1221(2)	6.3043(2)	319.7874
573 K	7.1250(2)	6.3106(2)	320.3570
673 K	7.1279(2)	6.3168(2)	320.9360
773 K	7.1308(2)	6.3229(2)	321.5063
873 K	7.1337(2)	6.3292(2)	322.0852
YV_{0.75}As_{0.25}O₄: 2% Eu³⁺	a [Å]	c [Å]	V [Å³]
298 K	7.1020(3)	6.2925(2)	317.3839
373 K	7.1029(3)	6.2959(3)	317.6416
473 K	7.1057(3)	6.3013(3)	318.1605
573 K	7.1079(4)	6.3071(3)	318.6486
673 K	7.1103(4)	6.3126(3)	319.1443
773 K	7.1134(4)	6.3184(4)	319.7148
873 K	7.1162(5)	6.3243(4)	320.2626
YV_{0.5}As_{0.5}O₄: 2% Eu³⁺	a [Å]	c [Å]	V [Å³]
298 K	7.0836(2)	6.2926(2)	315.7451
373 K	7.0851(2)	6.2957(2)	316.0328
473 K	7.0874(2)	6.3008(2)	316.4984
573 K	7.0898(2)	6.3052(2)	316.9296
673 K	7.0929(3)	6.3108(2)	317.4918
773 K	7.0956(3)	6.3159(2)	317.9867
873 K	7.0989(3)	6.3214(2)	318.5637
YV_{0.25}As_{0.75}O₄: 2% Eu³⁺	a [Å]	c [Å]	V [Å³]
298 K	7.0633(3)	6.2896(2)	313.7900
373 K	7.0647(3)	6.2926(2)	314.0625
473 K	7.0670(3)	6.2971(2)	314.4956
573 K	7.0700(3)	6.3021(2)	315.0120
673 K	7.0731(3)	6.3066(2)	315.5169
773 K	7.0762(3)	6.3114(2)	316.0286
873 K	7.0804(3)	6.3174(3)	316.7061

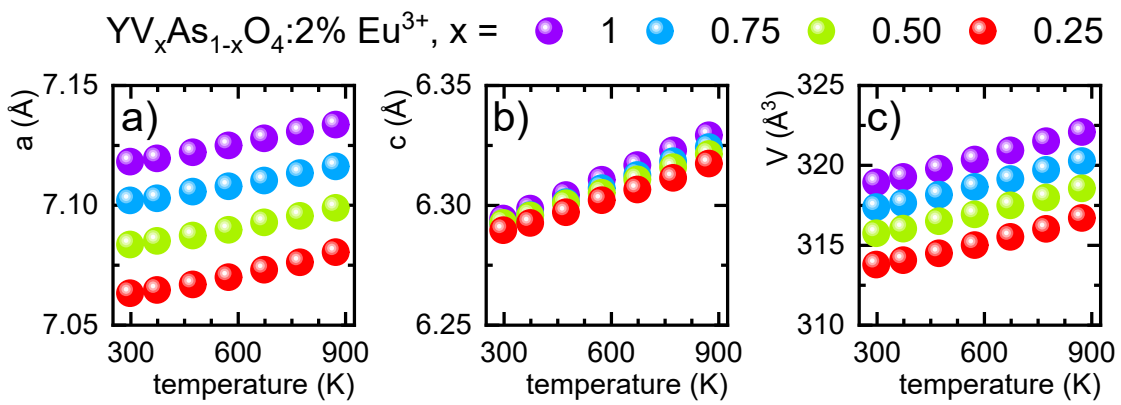


Figure S2. Thermal dependence of a – a) and c – b) unit cell parameters and the unit cell volume V in $\text{YV}_x\text{As}_{1-x}\text{O}_4:2\% \text{ Eu}^{3+}$ materials – c).

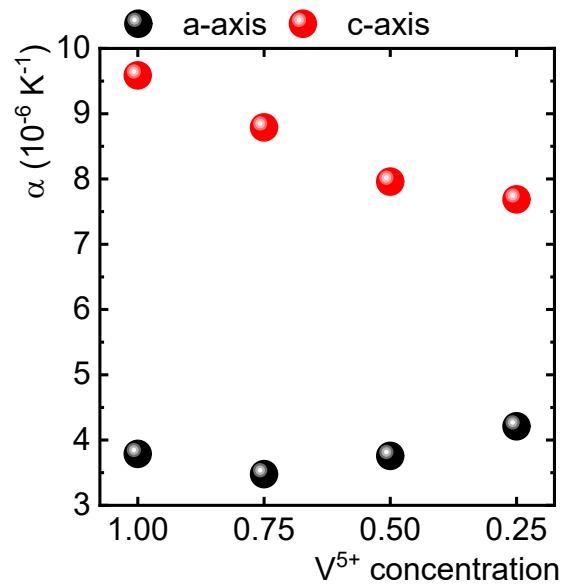


Figure S3. The influence of $\text{V}^{5+}/\text{As}^{5+}$ ratio on the thermal expansion coefficient along a-axis and c-axis in $\text{YV}_x\text{As}_{1-x}\text{O}_4:2\% \text{ Eu}^{3+}$ materials.

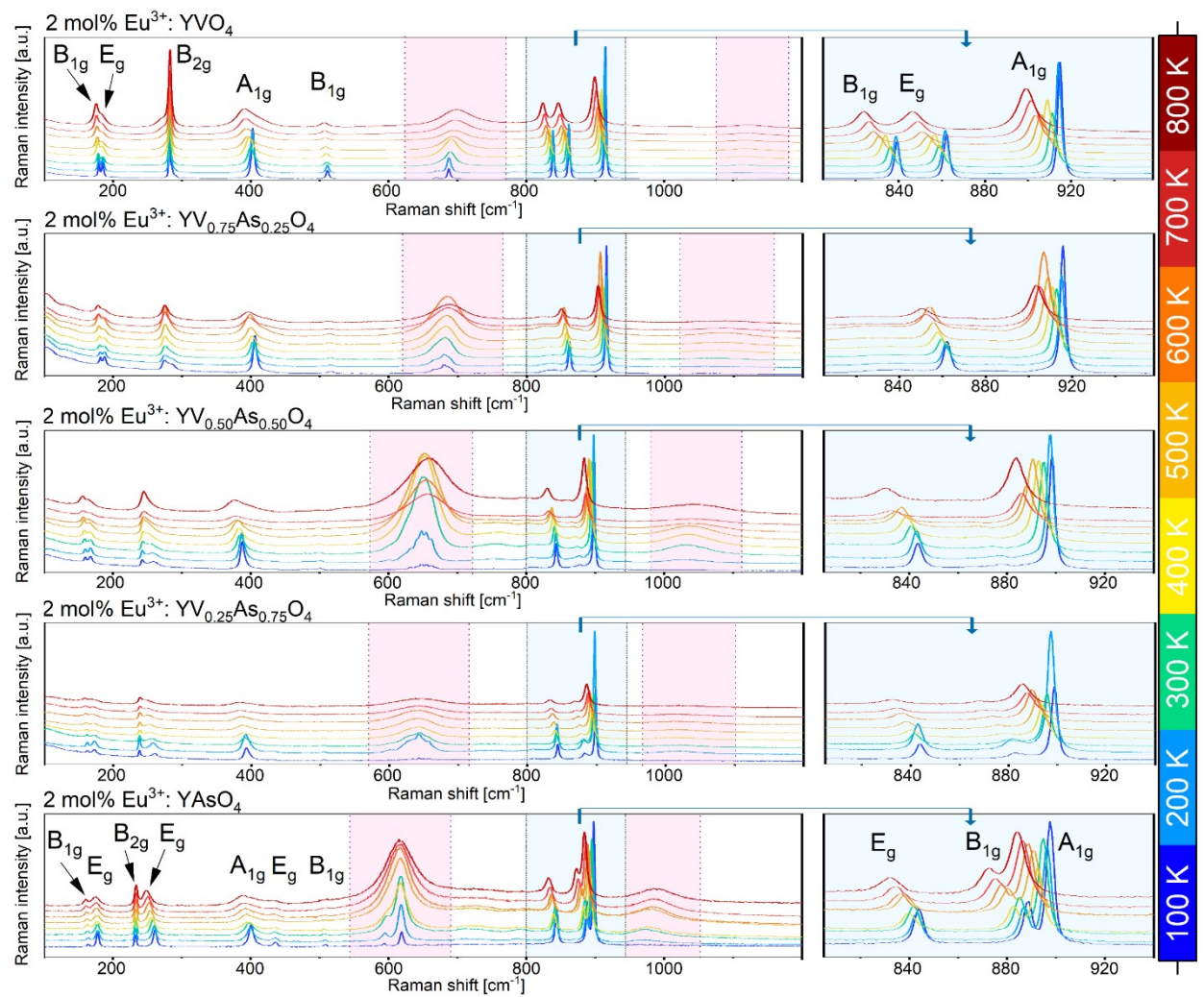


Figure S4. The Micro-Raman measurements obtained in the temperature range from 100 K to 800 K for 2 mol% Eu^{3+} -doped $\text{YV}_x\text{As}_{1-x}\text{O}_4$, where $x = 0, 0.25, 0.50, 0.75, 1$.

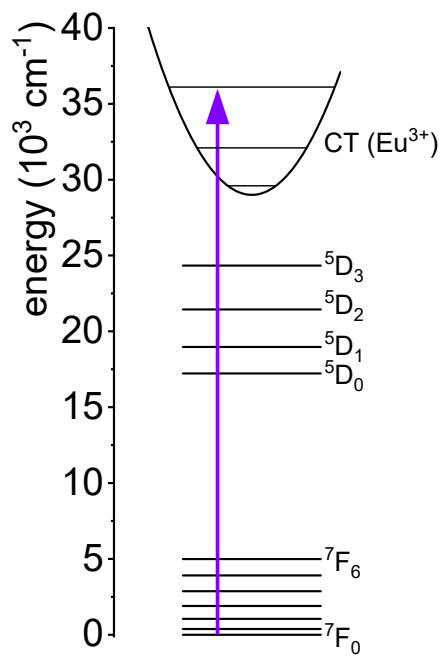


Figure S5. Energy level diagram of Eu³⁺ ions.

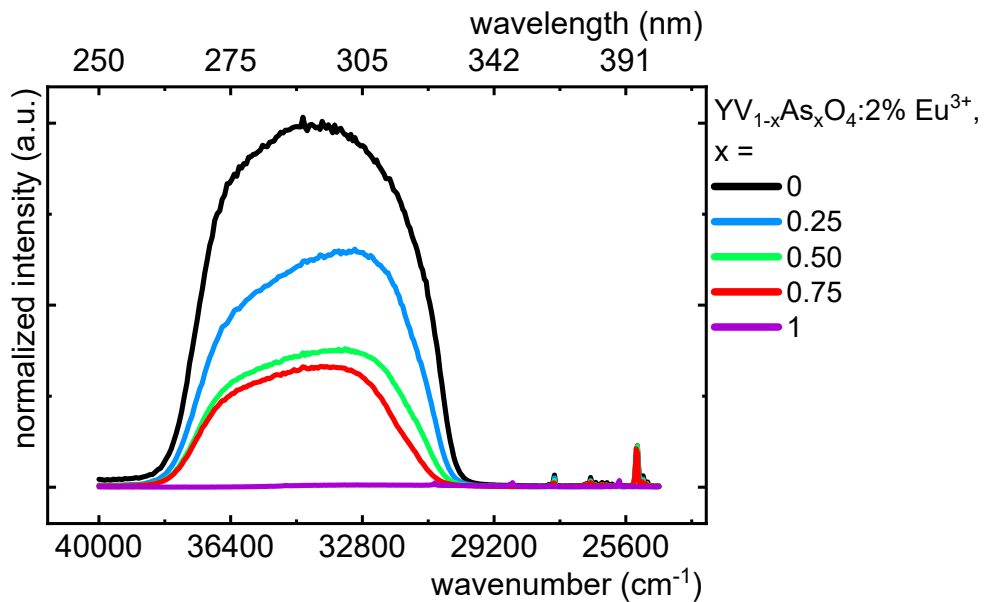


Figure S6. The comparison of the excitation spectra for YV_{1-x}As_xO₄:2% Eu³⁺ powders normalized to Eu³⁺ band correlated with $^7F_0 \rightarrow ^5L_6$ transition (395 nm, $\sim 25300 \text{ cm}^{-1}$) measured at 83 K.

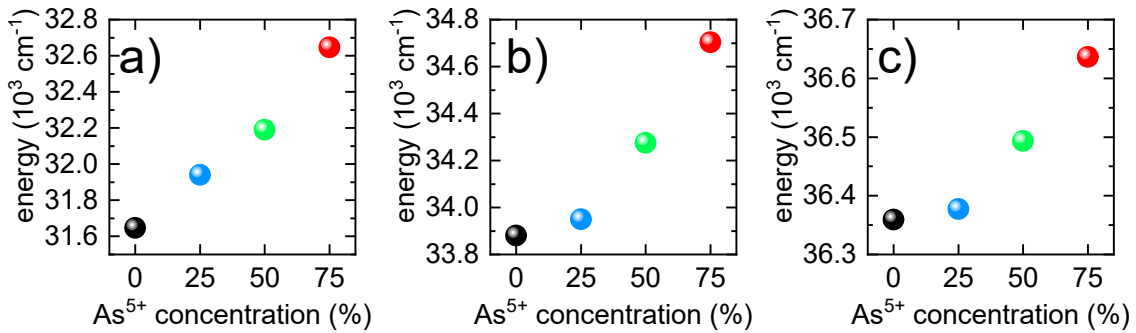


Figure S7. The influence of As⁵⁺ concentration on the spectral position of ${}^1\text{E}({}^1\text{T}_1)\rightarrow{}^1\text{B}_2({}^1\text{T}_2)$ – (a) and ${}^1\text{A}_2({}^1\text{T}_1)\rightarrow{}^1\text{B}_2({}^1\text{T}_2)$ excitation bands of VO₄³⁻ group – (b) and charge transfer O²⁻→Eu³⁺ (CT) band of Eu³⁺ ions – (c) for YV_{1-x}As_xO₄:2% Eu³⁺ powders at low temperature (83 K).

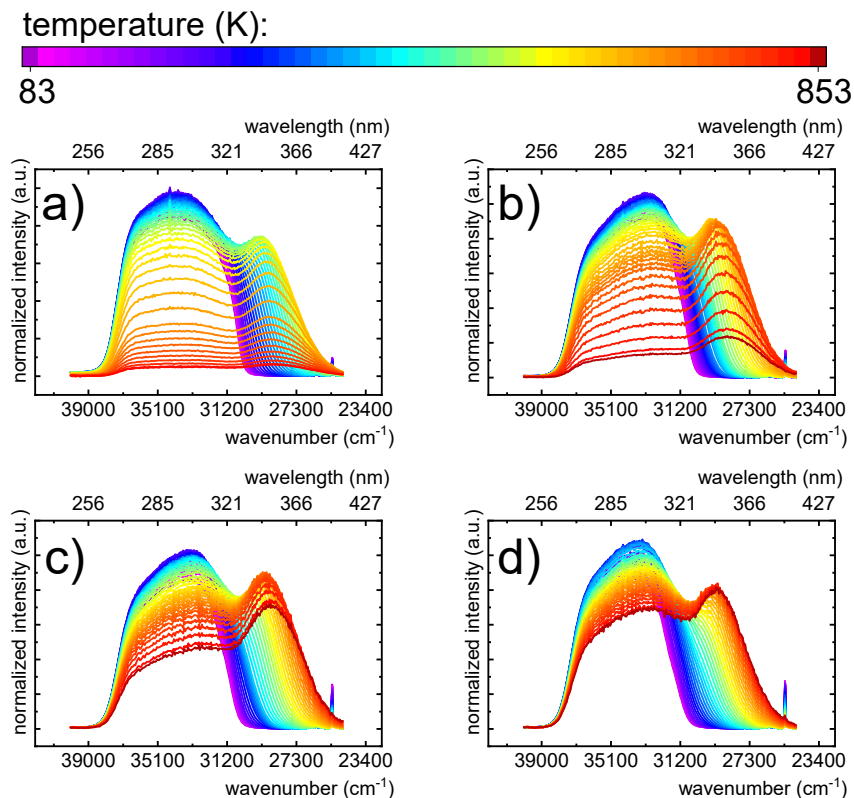


Figure S8. Thermal evolution of excitation spectra for YV_{1-x}As_xO₄:2% Eu³⁺ powders, where x = 0 (a), 0.25 (b), 0.50 (c), 0.75 (d).

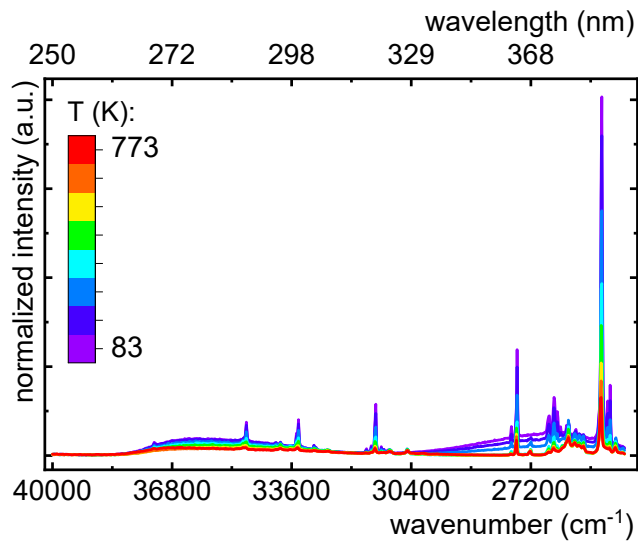


Figure S9. Thermal evolution of excitation spectra for $\text{YAsO}_4:2\% \text{Eu}^{3+}$ powder.

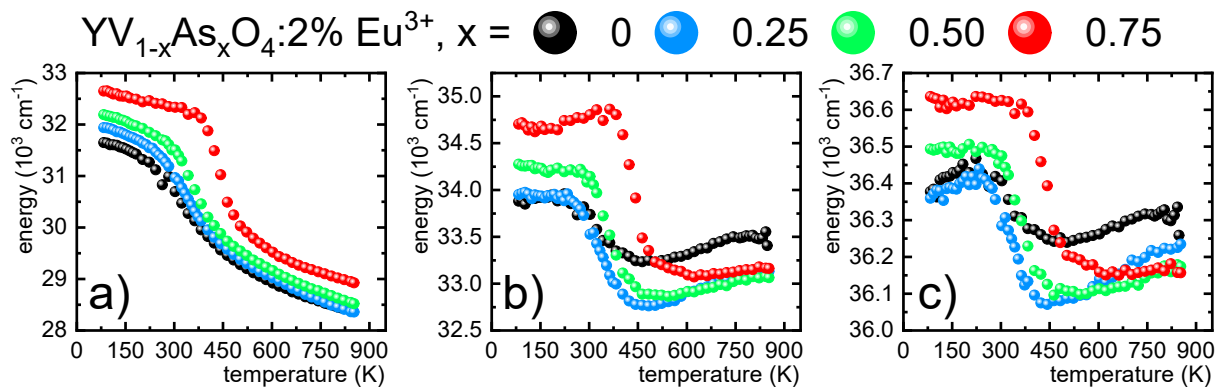


Figure S10. The thermal evolution of the spectral position of ${}^1\text{E}({}^1\text{T}_1) \rightarrow {}^1\text{B}_2({}^1\text{T}_2)$ (a) and ${}^1\text{A}_2({}^1\text{T}_1) \rightarrow {}^1\text{B}_2({}^1\text{T}_2)$ (b) excitation bands of VO_4^{3-} group (b) and charge transfer $\text{O}^{2-} \rightarrow \text{Eu}^{3+}$ (CT) band of Eu^{3+} ions (c) for $\text{YV}_{1-x}\text{As}_x\text{O}_4:2\%$ Eu^{3+} .

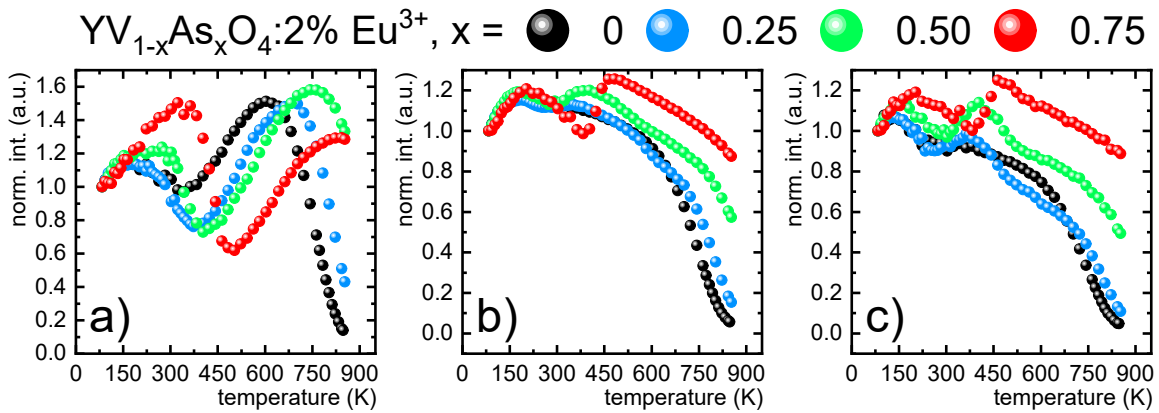


Figure S11. The thermal evolution of the band integral intensities of ${}^1\text{E}({}^1\text{T}_1)\rightarrow{}^1\text{B}_2({}^1\text{T}_2)$ (a) and ${}^1\text{A}_2({}^1\text{T}_1)\rightarrow{}^1\text{B}_2({}^1\text{T}_2)$ excitation bands of VO_4^{3-} group (b) and charge transfer $\text{O}^{2-}\rightarrow\text{Eu}^{3+}$ (CT) band of Eu^{3+} ions (c) for $\text{YV}_{1-x}\text{As}_x\text{O}_4:2\% \text{ Eu}^{3+}$.

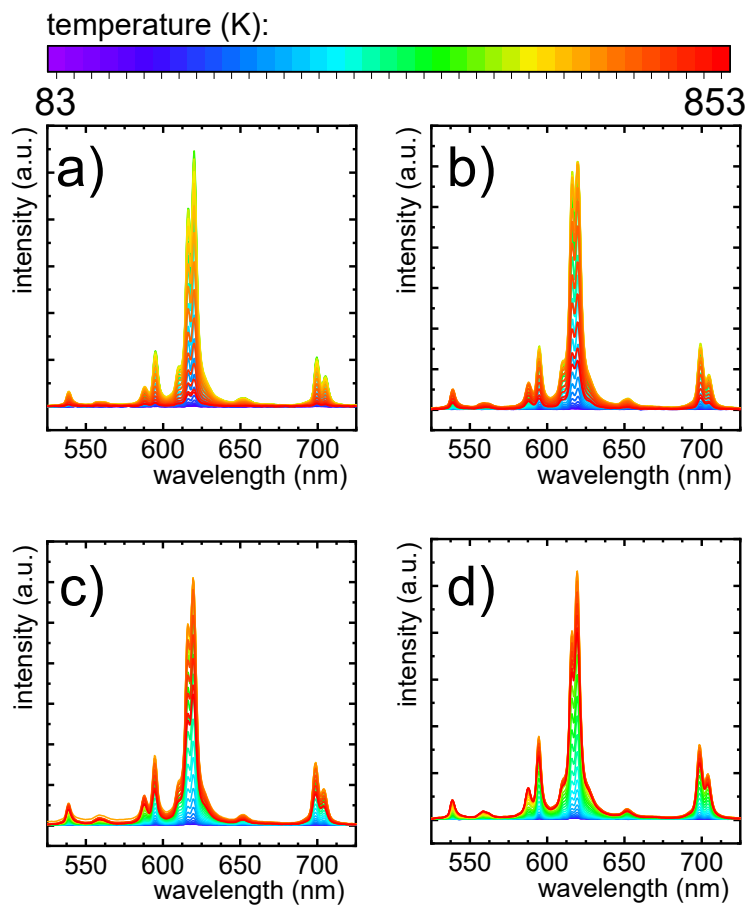


Figure S12. Thermal evolution of emission spectra excited by $\lambda_{\text{exc}} = 350 \text{ nm}$ for $\text{YV}_{1-x}\text{As}_x\text{O}_4:2\% \text{ Eu}^{3+}$ powders, where $x = 0$ (a), 0.25 (b), 0.50 (c), 0.75 (d).

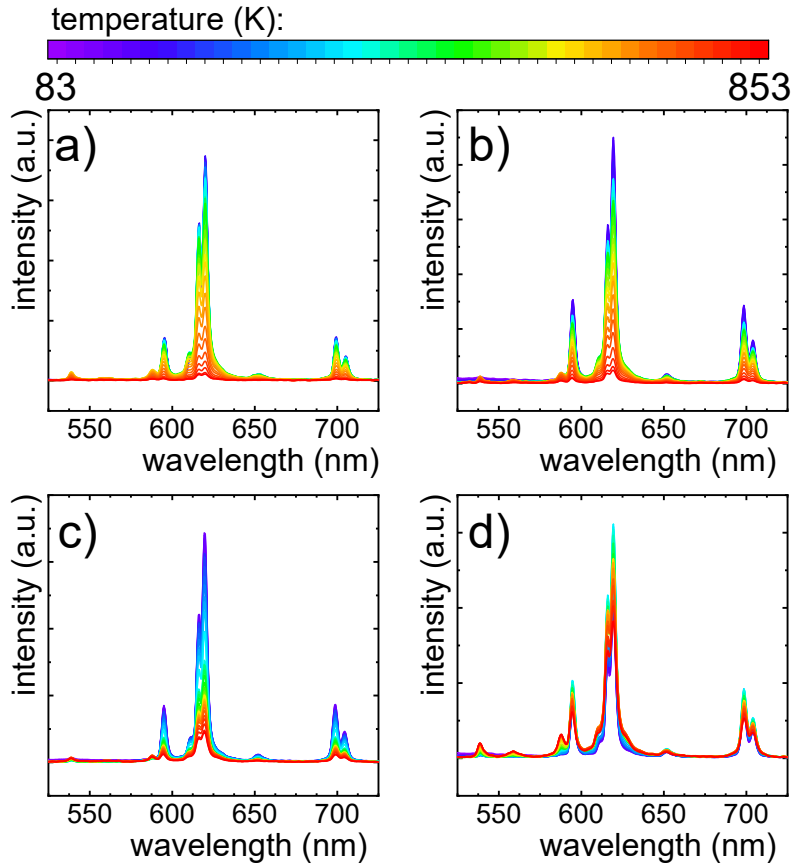


Figure S13. Thermal evolution of emission spectra excited by $\lambda_{\text{exc}} = 395 \text{ nm}$ for $\text{YV}_{1-x}\text{As}_x\text{O}_4:2\% \text{ Eu}^{3+}$ powders, where $x = 0$ (a), 0.25 (b), 0.50 (c), 0.75 (d).

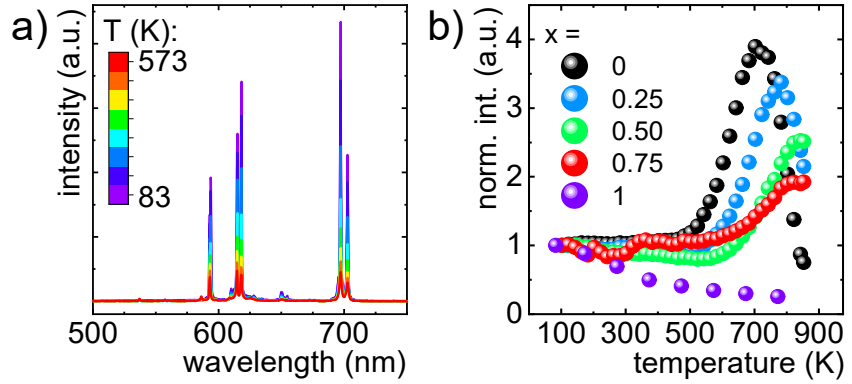


Figure S14. Thermal evolution of emission spectra excited by $\lambda_{\text{exc}} = 395 \text{ nm}$ for $\text{YAsO}_4:2\% \text{ Eu}^{3+}$ powder – a) and comparison of the thermal evolution of ${}^5\text{D}_0 \rightarrow {}^7\text{F}_2$ band intensities for $\text{YV}_{1-x}\text{As}_x\text{O}_4:2\% \text{ Eu}^{3+}$ and $\text{YAsO}_4:2\% \text{ Eu}^{3+}$ ($x = 1$) – b).

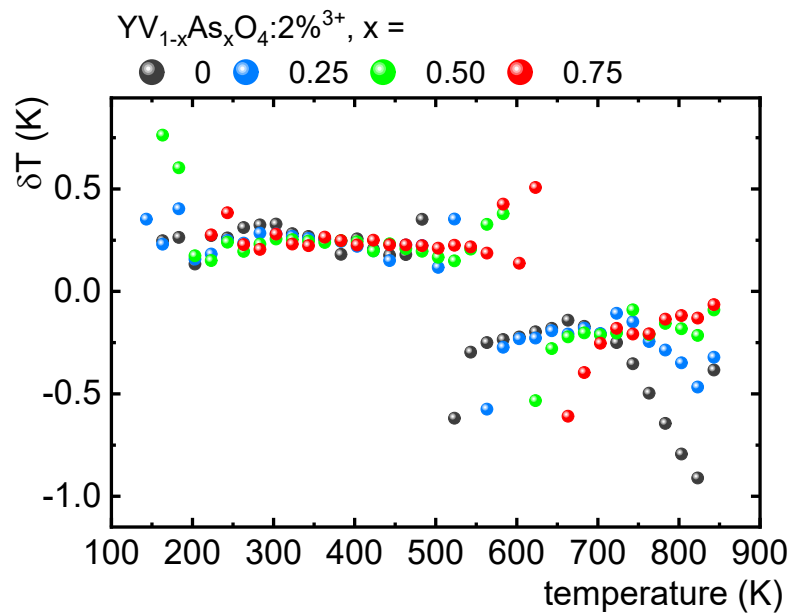


Figure S15. Thermal dependence of temperature estimation uncertainty of LIR($\lambda_{\text{exc}} = 350 \text{ nm}$ / $\lambda_{\text{exc}} = 395 \text{ nm}$) for YV_{1-x}As_xO₄:2% Eu³⁺.

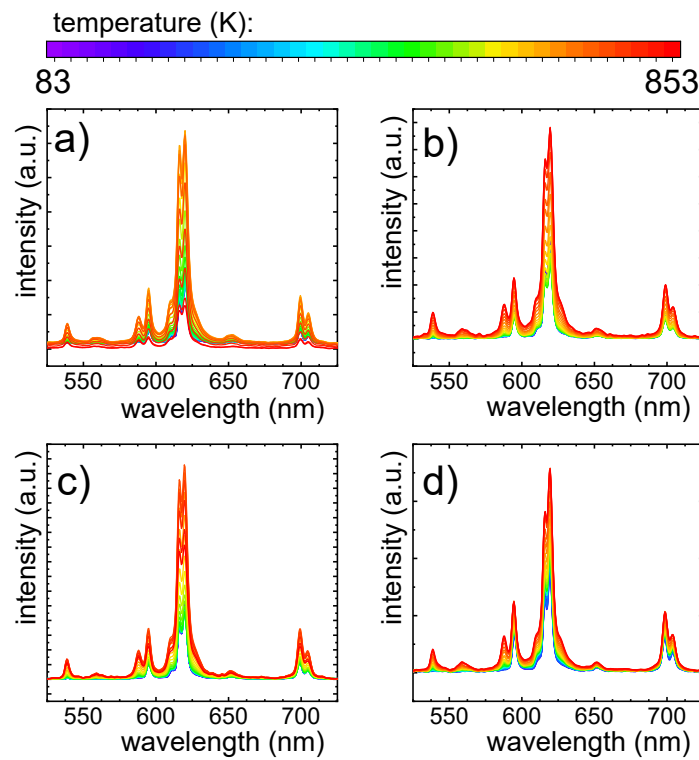


Figure S16. Thermal evolution of emission spectra excited by $\lambda_{\text{exc}} = 290$ nm for $\text{YV}_{1-x}\text{As}_x\text{O}_4:2\%$ Eu^{3+} powders, where $x = 0$ (a), 0.25 (b), 0.50 (c), 0.75 (d).

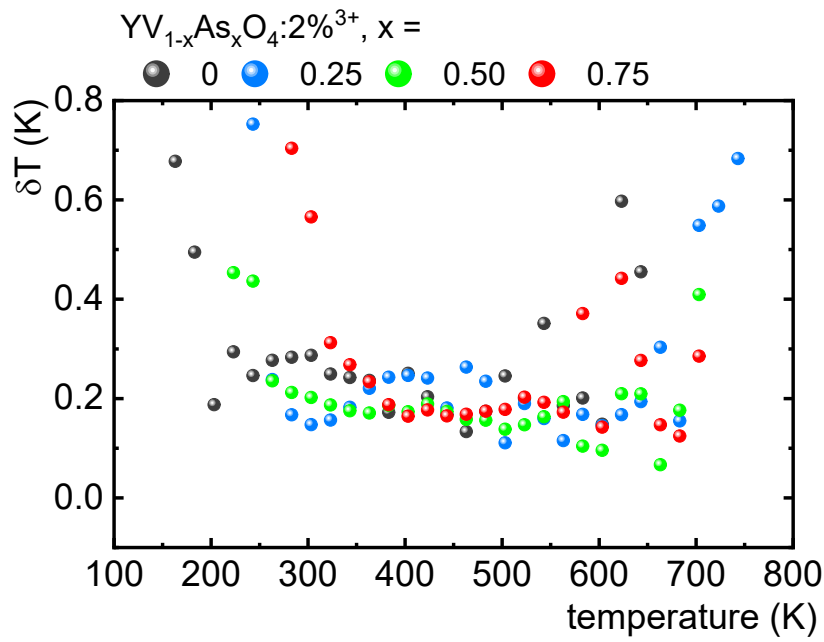


Figure S17. Thermal dependence of temperature estimation uncertainty of LIR($\lambda_{\text{exc}} = 350 \text{ nm} / \lambda_{\text{exc}} = 290 \text{ nm}$) for

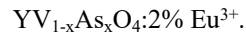


Table S2. Comparison of thermometric parameters of the investigated $\text{YV}_x\text{As}_{1-x}\text{O}_4$ materials with Eu^{3+} luminescence-based materials reported in the literature.

Host material	thermometric mode with details	$S_{R\max}$	$T(S_{R\max})$	temperature range	Ref
		(%K ⁻¹)	(K)	with $S_R > 1\% \text{K}^{-1}$ (K)	
CsPbBr_3	$\text{LIR} = I(^5\text{D}_0 \rightarrow ^7\text{F}_2)/I_{\text{QD}}$	2.25	312	$\sim 230 - 400$	[1]
ScVO_4	$I(^5\text{D}_0 \rightarrow ^7\text{F}_4)$	7.19	113	113 - 300	[2]
GdAlO_3	$\tau(^5\text{D}_0)$	2.28	793	$\sim 725 - 793$	[3]
LiYO_2	$\text{LIR} = I(^5\text{D}_0 \rightarrow ^7\text{F}_1)(T(0 \rightarrow 1))$ $/I(^5\text{D}_0 \rightarrow ^7\text{F}_1)(M(0 \rightarrow 2))$	11.8	295	250-303	[4]
NaYF_4	$\text{LIR} = I(^5\text{D}_0 \rightarrow ^7\text{F}_4)(\lambda_{\text{exc}} = \text{ESA})$ $/I(^5\text{D}_0 \rightarrow ^7\text{F}_4)(\lambda_{\text{exc}} = \text{GSA})$	4.11	213	$\sim 200 - 400$	[5]
NaGdF_4	$\text{LIR} = I(^5\text{D}_0 \rightarrow ^7\text{F}_4) (\lambda_{\text{exc}} = \text{ESA})$ $/I(^5\text{D}_0 \rightarrow ^7\text{F}_4) (\lambda_{\text{exc}} = \text{GSA})$	16.9	163	$\sim 200 - 300$	[5]
$\text{Y}_3\text{Al}_5\text{O}_{12}$	$\text{LIR} = I(^5\text{D}_0 \rightarrow ^7\text{F}_4) / I(\text{Ti}^{3+} \rightarrow \text{O}^{2-})$	1.37	386	$\sim 290 - 470$	[6]

$\times(\text{Ti}^{3+})$

Y_2O_3	$\text{LIR} = \frac{\text{I}(\text{Er}^{3+})}{\text{I}(\text{Ti}^{3+})}$	1.4	303	303 - 410	[7]
GdNbO_4	$\text{LIR} = \frac{\text{I}(\text{Bi}^{3+})}{\text{I}(\text{Ti}^{3+})}$	3.81	300	300-525	[8]
YVO_4	$\text{LIR} = \frac{\text{I}(\text{host})}{\text{I}(\text{Ti}^{3+})}$	4.5	123	123 - 323	[9]
YVO_4	$\text{LIR} = \frac{\text{I}(\text{D}_1 \rightarrow \text{F}_1)}{\text{I}(\text{D}_0 \rightarrow \text{F}_1)}$	~ 2.7	300	300 - 500	[10]
YVO_4	$\text{LIR} = \frac{\text{I}(\text{D}_1 \rightarrow \text{F}_1)}{\text{I}(\text{D}_0 \rightarrow \text{F}_4)}$	~ 0.62	~ 500	-	[11]
YVO_4	$\text{LIR} = \frac{\text{I}(\text{D}_0 \rightarrow \text{F}_2)(\lambda_{\text{exc}}=342 \text{ nm})}{\text{I}(\text{D}_0 \rightarrow \text{F}_2)(\lambda_{\text{exc}}=266 \text{ nm})}$	3.0	233	183-348	[12]
YVO_4	$\text{LIR} = \frac{\text{I}(\text{D}_0 \rightarrow \text{F}_2)(\lambda_{\text{exc}}=350 \text{ nm})}{\text{I}(\text{D}_0 \rightarrow \text{F}_2)(\lambda_{\text{exc}}=395 \text{ nm})}$	2.55	233	175-413	This work
$\text{YV}_{0.25}\text{As}_{0.75}\text{O}_4$	$\text{LIR} = \frac{\text{I}(\text{D}_0 \rightarrow \text{F}_2)(\lambda_{\text{exc}}=350 \text{ nm})}{\text{I}(\text{D}_0 \rightarrow \text{F}_2)(\lambda_{\text{exc}}=395 \text{ nm})}$	1.66	335	270-486	This work
$\text{YV}_{0.75}\text{As}_{0.25}\text{O}_4$	$\text{LIR} = \frac{\text{I}(\text{D}_0 \rightarrow \text{F}_2)(\lambda_{\text{exc}}=350 \text{ nm})}{\text{I}(\text{D}_0 \rightarrow \text{F}_2)(\lambda_{\text{exc}}=290 \text{ nm})}$	4.05	293	250-416	This work
$\text{YV}_{0.25}\text{As}_{0.75}\text{O}_4$	$\text{LIR} = \frac{\text{I}(\text{D}_0 \rightarrow \text{F}_2)(\lambda_{\text{exc}}=350 \text{ nm})}{\text{I}(\text{D}_0 \rightarrow \text{F}_2)(\lambda_{\text{exc}}=290 \text{ nm})}$	2.02	387	315-516	This work

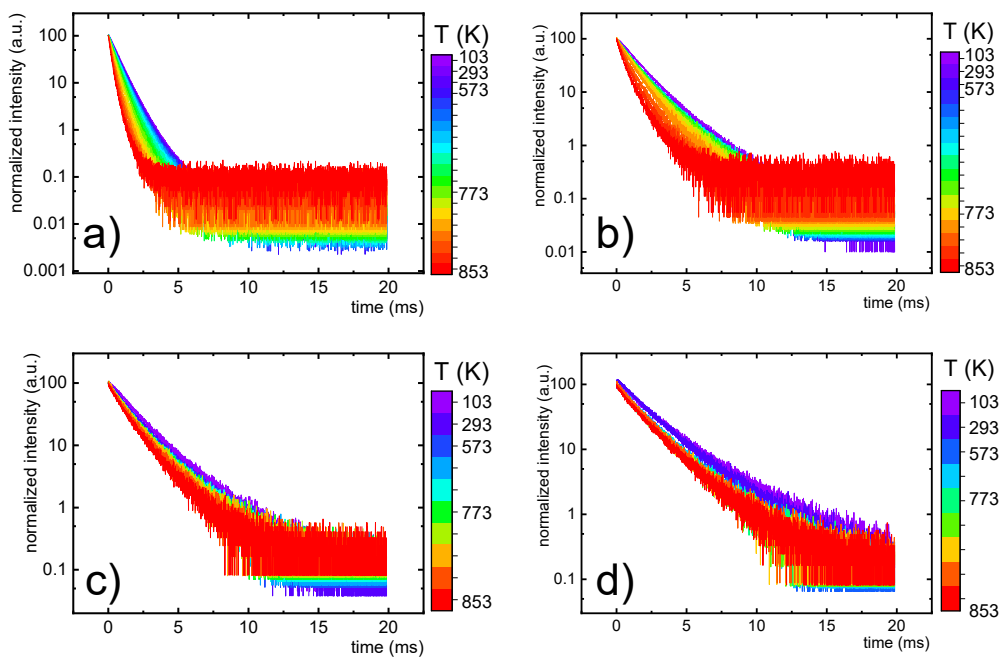


Figure S18. Thermal evolution of the luminescent decays of Eu^{3+} excited states for $\text{YV}_{1-x}\text{As}_x\text{O}_4:2\%$ Eu^{3+} powders, where $x = 0$ (a), 0.25 (b), 0.50 (c), 0.75 (d).

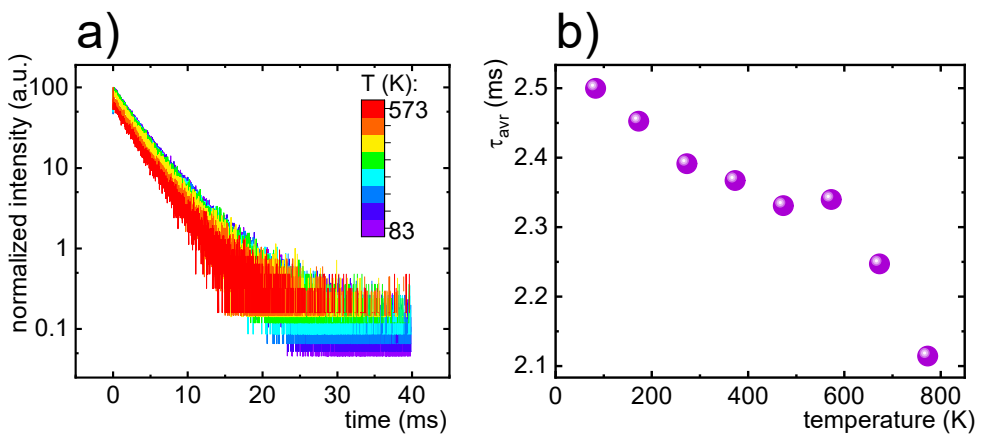


Figure S19. Thermal evolution of the luminescent decays – a) and the average lifetimes of Eu^{3+} excited states for $\text{YAsO}_4:2\%$ Eu^{3+} powder – b).

References

- [1] X. Li, Y. Yu, J. Hong, Z. Feng, X. Guan, D. Chen, Z. Zheng, Optical temperature sensing of Eu³⁺-doped oxyhalide glasses containing CsPbBr₃ perovskite quantum dots, *J. Lumin.* 219 (2020) 116897.
- [2] M.T. Abbas, N.Z. Khan, N. Muhammad, I. Mehmood, J. Mao, S.A. Khan, Temperature sensing performance of ScVO₄: Eu³⁺ phosphors by employing ground state thermal coupling approach, *J. Alloys Compd.* 906 (2022) 164340.
- [3] V. Lojpur, S. Ćulubrk, M. Medić, M. Dramicanin, Luminescence thermometry with Eu³⁺ doped GdAlO₃, *J. Lumin.* 170 (2016) 467–471.
- [4] L. Marciniak, W. Piotrowski, M. Szalkowski, V. Kinzhylbalo, M. Drozd, M. Dramicanin, A. Bednarkiewicz, Highly sensitive luminescence nanothermometry and thermal imaging facilitated by phase transition, *Chem. Eng. J.* 427 (2022) 131941.
- [5] K. Trejgis, K. Ledwa, A. Bednarkiewicz, L. Marciniak, Impact of host composition and dopant ion concentration on the thermometric properties of a Eu³⁺ activated fluoride-based single-band ratiometric luminescent thermometer, *J. Alloys Compd.* 898 (2022) 162839..
- [6] J. Drabik, L. Marciniak, The influence of Eu³⁺ concentration on the spectroscopic properties of YAG:Ti, Eu³⁺ nanocrystalline luminescent thermometer, *J. Lumin.* 208 (2019) 213–217.
- [7] M.D. Rabasović, B.D. Murić, V. Čelebonović, M. Mitrić, B.M. Jelenković, M.G. Nikolić, Luminescence thermometry via the two-dopant intensity ratio of Y₂O₃:Er³⁺, Eu³⁺, *J. Phys. D. Appl. Phys.* 49 (2016) 485104.
- [8] J. Xue, H.M. Noh, B.C. Choi, S.H. Park, J.H. Kim, J.H. Jeong, P. Du, Dual-functional

of non-contact thermometry and field emission displays via efficient $\text{Bi}^{3+} \rightarrow \text{Eu}^{3+}$ energy transfer in emitting-color tunable GdNbO_4 phosphors, *Chem. Eng. J.* 382 (2020) 122861.

- [9] I.E. Kolesnikov, D. V Mamonova, M.A. Kurochkin, E.Y. Kolesnikov, E. Lähderanta, Optical Thermometry by Monitoring Dual Emissions from YVO_4 and Eu^{3+} in $\text{YVO}_4:\text{Eu}^{3+}$ Nanoparticles, *ACS Appl. Nano Mater.* 4 (2021) 1959–1966.
- [10] I.E. Kolesnikov, A.A. Kalinichev, M.A. Kurochkin, D. V Mamonova, E.Y. Kolesnikov, E. Lähderanta, Ratiometric Optical Thermometry Based on Emission and Excitation Spectra of $\text{YVO}_4:\text{Eu}^{3+}$ Nanophosphors, *J. Phys. Chem. C.* 123 (2019) 5136–5143.
- [11] A. Ćirić, S. Stojadinović, M.D. Dramićanin, Time-integrated luminescence thermometry of Eu^{3+} and Dy^{3+} doped YVO_4 , *Sensors Actuators A Phys.* 295 (2019) 450–455.
- [12] W. Piotrowski, L. Dalipi, K. Elzbieciak-Piecka, A. Bednarkiewicz, B. Fond, L. Marciniak, Self-Referenced Temperature Imaging with Dual Light Emitting Diode Excitation and Single-Band Emission of $\text{AVO}_4:\text{Eu}^{3+}$ ($\text{A}=\text{Y}, \text{La}, \text{Lu}, \text{Gd}$) Nanophosphors , *Adv. Photonics Res.* 3 (2022) 2100139.